



# Synthesis and characterization of cadmium doped on ZnO thin films prepared by SILAR method for photocatalytic degradation properties of MB under UV irradiation

M. Sathya<sup>1</sup>, G. Selvan<sup>1</sup>, M. Karunakaran<sup>2,a</sup> , K. Kasirajan<sup>3</sup>, S. Usha<sup>2</sup>, M. Logitha<sup>2</sup>, S. Prabakaran<sup>2</sup>, P. Baskaran<sup>4</sup>

<sup>1</sup> Department of Physics, Thanthai Hans Roever College (Autonomous), Perambalur, Affiliated to Bharathidasan University, Trichy 621 220, India

<sup>2</sup> Thin Film and Nanoscience Research Lab, Department of Physics, Alagappa Government Arts College, Karaikudi 621 220, India

<sup>3</sup> Division of Advanced Materials Engineering, Kongju National University, Budaedong 275, Seobuk-gu, Cheonan-si, Chungnam 31080, Republic of Korea

<sup>4</sup> Department of Physics, Government Arts and Science College, Veppanthattai, Perambalur 621 116, India

Received: 9 May 2022 / Accepted: 5 January 2023

© The Author(s), under exclusive licence to Società Italiana di Fisica and Springer-Verlag GmbH Germany, part of Springer Nature 2023

**Abstract** The presented manuscript deals with the synthesis of uniformly coated nanocrystalline ZnO and Cd-doped ZnO thin films with various concentrations (1, 3, and 5 wt%) via the successive ionic layer adsorption and reaction (SILAR) method. The physical and chemical attributes of the prepared films were examined through certain analytical techniques such as XRD, SEM with EDS, UV, PL, and RAMAN spectroscopy. The XRD, SEM, and Raman results confirmed that Cd is successfully incorporated on the surface of ZnO. The optical properties of the films were analyzed from absorption studies of Cd:ZnO thin films. Furthermore, the estimated optical band gap values of the Cd:ZnO films decrease from 3.03 to 2.95 eV. The photocatalytic properties of the synthesized ZnO and Cd:ZnO thin films were investigated against the methylene blue (MB) under UV light irradiation. The results of methylene blue photodegradation reached (49.6%) for ZnO films and (55.2%, 71.4%, and 82.5%) for Cd:ZnO films. Finally, this research suggests that the Cd:ZnO films exhibit better photocatalytic efficiency compared to the ZnO films.

## 1 Introduction

Photocatalysis is an efficient method for degrading pollutants that makes use of inexhaustible and clean solar energy. In particular, the photocatalysis process is the simplest low cost and eco-friendly technique compared to others [1–3]. In this process, the required radicals are produced by the oxidation and reduction process with the help of holes and electrons present on the surface of the photocatalysts [4–7]. The formed radicals then react with the organic bond of the effluent, resulting in the mineralized harmless components. Semiconductor photocatalysis is one of the most advanced physicochemical processes used in the photodegradation of environmental pollutants and toxic compounds. Scientists have made efforts to improve highly efficient semiconductor photocatalysts such as TiO<sub>2</sub>, SnO<sub>2</sub>, ZnO, CuO, WO<sub>3</sub>, etc. [8–10]. Further, TiO<sub>2</sub> and ZnO are considered the most abundant semiconductor photocatalysts materials. Zinc oxide (ZnO) has higher photocatalytic efficiency than titanium dioxide and is more biocompatible and stable in the environment. ZnO can replace TiO<sub>2</sub> due to its physicochemical properties, as well as its band gap [11–14].

ZnO is an n-type semiconductor that belongs to the II–VI group of semiconductors. ZnO is a multifunctional metal oxide semiconductor material widely applied in the photocatalysis process because it has a direct wide range of optical band gap values (~3.37 eV) with high excitation of binding energy (~60 meV) at room temperature [15, 16]. ZnO can be used in a variety of applications including pigments, gas sensors, optical devices, solar cells, and photocatalysis. ZnO exhibits low efficiency under UV light irradiation because of its wide band gap. To overcome this limitation, ZnO is modified by several approaches, including controlling the morphology, size, and doping with various elements. The doping process can tune the optical and catalytic properties, and the ZnO band gap generates intragap electronic states inside the semiconductor. There are various transition metal available for tuning the suitable band gap of the ZnO nanostructure such as Ag, Cu, Fe, Pd, Cd, Mg, Ni, Gd, Sr, Au, and Al [17–20]. Among others, Cd (cadmium) is one of the most interesting elements due to its different electronic shell structures and larger ionic size than Zn. As a result, it could be considered promising candidate for modifying the structural, optical, physical, and chemical properties of ZnO [21].

Various methodologies have been proposed for the manufacture of ZnO thin film-like as sol–gel, RF magnetron sputtering, successive ionic layer adsorption and reaction (SILAR), pulsed deposition, and spray pyrolysis [22, 23]. Among these methods,

Focus Point on Rarefied Flows at Micro- and Nano-Scale. Guest editors: A. Karimipour, K. Hooman, A. D’Orazio, R. Kalbasi.

<sup>a</sup> e-mail: tvdkaruna@gmail.com (corresponding author)

SILAR is a solution-based technique that has many advantages such as being simple, safe, environmentally friendly, and low cost. In the SILAR method, to remove the loosely bound species, the substrate is soaked separately into two precursor solutions and then rinsed with water. As a result, one SILAR cycle involves the adsorption of the cation precursor, rinsing with water, the adsorption of the anion precursor, reaction, and another rinse. This technique is also capable of producing metal oxide films at relatively low temperatures [24]. Herein, we are reporting a synthesis and characterization of ZnO and Cd:ZnO thin films with various concentrations through in-depth studies based on their structural, morphological and optical properties. Finally, the as-prepared Cd:ZnO films show enhanced performance for photocatalysis applications when compared with their pure ZnO counterpart. In this case, methylene blue (MB) dye is used as effluent throughout the entire process.

## 2 Experimental procedure

### 2.1 Materials

All of the chemicals were analytical grade (AR) reagents that were used exactly as they were obtained, without any kind of processing. Zinc sulfate ( $\text{ZnSO}_4$ ), sodium hydroxide (NaOH), and dopant cadmium chloride ( $\text{CdCl}_2$ ) were purchased from Sigma Aldrich (India). Deionized water has been utilized as a solvent during the entire manufacturing process.

### 2.2 Synthesis of ZnO and Cd:ZnO thin films

In our experiment, the uniformly coated ZnO and Cd:ZnO thin films with various incorporation of Cd (1, 3, and 5 wt%) were synthesized by using a modified SILAR technique. Before starting the fabrication, the glass substrate was cleaned with the help of chromic acid, double-distilled water, and acetone. To make a homogeneous sodium zincates precursor, dissolve 0.1 M zinc sulfate and 0.2 M NaOH in 50-ml double-distilled water and then stirred vigorously for 30 min. Usually, the standard SILAR method consists of four beakers system but this modified SILAR consists of two beakers only. The precursor solution at one beaker and the next one contain hot water to eliminate the unpacked ions in the formed films and are kept at a temperature of nearly 90 °C. The glass substrate was vertically immersed in the sodium zincate bath for 30 s and then submerged in hot water (90 °C) for 10 s to eliminate the loosely adsorbed ions. A similar approach has been used for ~80 dipping cycles to ensure pristine ZnO film. For Cd:ZnO thin films, similar approaches have been used to form zinc complex solution with the addition of cadmium chloride with various concentrations 1, 3, and 5 wt%, respectively. Finally, the prepared thin films were dried and annealed for 2 h at 300 °C. After the annealing process, the resulted thin films carry out for further testing to confirm the incorporation of Cd in the prepared films.

### 2.3 Characterization tools

Various instrumentation techniques were used to examine the fundamental behavior and characteristics of the synthesized film. The crystallographic data and structural details of the as-prepared ZnO and Cd:ZnO thin films were recorded using PAN analytical X'pert PRO X-ray diffraction (XRD) system with a Cu  $K\alpha$  wavelength ( $\lambda = 1.5405 \text{ \AA}$ ) by varying  $2\theta$  from 10 to 80°, were operated at a voltage of 36 kV and 18 mA current. The shape and surface morphology of samples were examined by the JEOL JSM 5800 LV scanning electron microscope (SEM) instrument operating at an accelerating voltage of 20 kV and the presence of elements was investigated with the help of EDX system (SU-70, Hitachi) while the component distribution was assessed by the Elemental mapping analysis using XL G2 Desktop Scanning Electron Microscope. The absorbance and transmittance spectra of the samples were recorded in the wavelength range between 350 and 900 nm with a step resolution of 2.5 nm by using UV–Visible spectrophotometer (UV–vis, JMNU-3010). Raman spectroscopy of synthesized films was carried out using Imaging Spectrograph STR 500 mm Focal Length Laser Raman spectrometer Flat field: 27 mm(W) × 14 mm (H), with a resolution of  $1/0.6 \text{ cm}^{-1}/\text{pixel}$  at the excitation wavelength of 488 nm. Photoluminescence (PL) emission spectra were recorded using the Oxford Low-temperature LN2 77 K spectrometer with an excitation wavelength of 325 nm.

### 2.4 Photocatalytic study

The photocatalytic activity of the samples was investigated by observing the photocatalytic dye degradation of model organic pollutants MB under visible light irradiation from a 50 W tungsten halogen lamp. The Cd:ZnO catalysts with 0, 1, 3, and 5 wt% Cd doping concentrations were immersed in four sets of aqueous solution (10 mL) containing 0.025 M MB dye. The thin films were immersed in the solution and kept in the dark for 30 min. This was done to reach an adsorption–desorption equilibrium. After every 30 min of exposure, 5 mL of the solution was collected for the study. This experiment was carried out for both pure ZnO and Cd-doped ZnO films. The UV–visible spectra were recorded until the complete degradation of the MB dye occurred. As irradiation time rises, the characteristic absorption peak intensity of MB (664 nm) is reduced.

**Table 1** The estimated values of crystalline size, strain, dislocation density, number of crystallites, and lattice constants for ZnO and Cd:ZnO thin films

Cd concentration (wt%)	Lattice constants (Å)		Film thickness (nm)	Crystallite size (nm)	Dislocation density ( $\times 10^{15}$ lines $m^{-2}$ )	Strain ( $\times 10^{-3}$ )	Number of crystallites ( $\times 10^{16} m^{-2}$ )	Band gap (eV)
	<i>a</i>	<i>c</i>						
0	3.0130	5.2188	920	45	0.4874	2.59	0.990	3.03
1	3.0068	5.2079	830	47	0.4467	2.48	0.783	3.00
3	3.0123	5.2175	815	50	0.4008	2.35	0.654	2.96
5	3.0094	5.2124	790	51	0.3822	2.29	0.590	2.95

### 3 Result and discussion

#### 3.1 X-ray diffraction studies

The XRD examinations carry out for the undoped and doped ZnO thin films with the  $2\theta$  (diffracting angle) ranging from 20 to 80° with  $CuK\alpha$  radiation ( $\lambda = 1.5406 \text{ \AA}$ ) are reflected in Fig. 1. Here, eight unique XRD peaks can be seen, corresponding to planes (100), (002), (101), (102), (110), (103), (112), and (201), respectively. Among them, the (002) plane is referred to as the preferential orientation peak with low surface energy. All of the identified diffraction peaks are hexagonal wurtzite with the space group P63mc, as confirmed by the correspondence with the standard JCPDS card no (36-1451) [25]. No additional peaks of dopants that could be attributable to the low dopant level were found. Another interesting observation in comparison with undoped ZnO is the peak shifting and extension of doped samples. The peak shift to higher angles in doped samples indicates that  $Zn^{2+}$  ions with lower ionic radii (0.74 Å) are replaced by dopant ions with larger ionic radii ( $Cd^{2+} \sim 0.96 \text{ \AA}$ ) [26]. Peak shifting could suggest that the  $Cd^{2+}$  ions have successfully occupied the crystallographic positions of  $Zn^{2+}$  ions in the ZnO host lattice and strain has developed in the lattice. The crystallite size of the synthesized films was estimated by using Debye–Scherer’s formula [27],

$$D = \frac{0.9\lambda}{\beta \cos \theta} \tag{1}$$

where  $\theta$ —Bragg’s diffraction angle,  $\beta$ —the full width at half maximum of the required diffraction lines,  $\lambda$ —X-ray wavelength of the spectrum ( $\sim 0.154 \text{ nm}$ ), and  $k$ —is the shape factor ( $\sim 0.9$ ). The average crystallite size of the ZnO and Cd:ZnO thin films with different Cd concentrations (1 wt%, 3 wt%, and 5 wt%) is shown in Table 1. The average crystallite size of pure ZnO is 45 nm. It is observed that the crystallite size increases with an increase in Cd doping concentration. This is due to the direct fact that the atomic radius of Cd is larger than the atomic radius of Zn. The following relations were used to calculate the structural parameters such as strain ( $\epsilon$ ), dislocation density ( $\delta$ ), and the number of crystallites ( $N$ ) [28]

$$\delta = \frac{1}{D^2} \tag{2}$$

$$\epsilon = \frac{\beta \cot \theta}{4} \tag{3}$$

$$N = \frac{t}{D^3} \tag{4}$$

where  $\beta$ —is the full width at half maximum,  $t$  is the film thickness, and  $D$  is the crystallite size. It is observed that the dislocation density, strains, and the number of crystallites gradually decrease with the increase of the Cd concentration. Further, the lattice constants ‘ $a$ ’ and ‘ $c$ ,’ as well as the unit cell volume ‘ $V$ ,’ of the film have been evaluated by using this relationship [29]

$$V = a^2c(\sin 60^\circ) \tag{5}$$

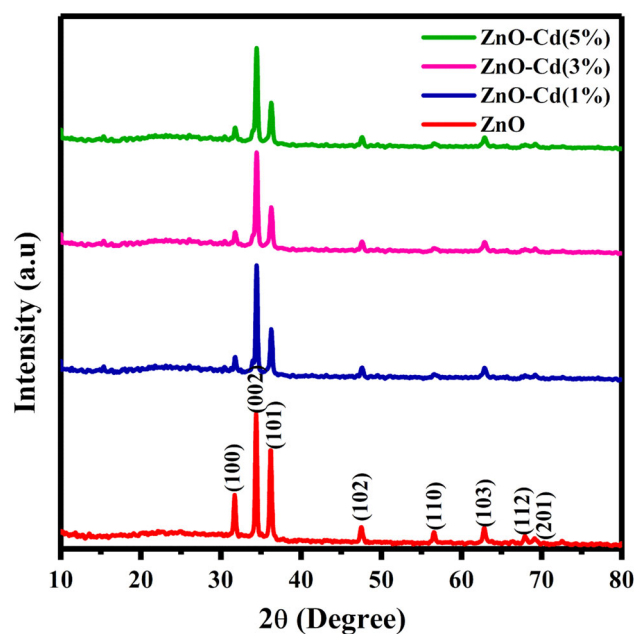
$$\frac{1}{d^2} = \frac{4}{3} \left\{ \frac{h^2 + hk + k^2}{a^2} \right\} + \left\{ \frac{l^2}{c^2} \right\} \tag{6}$$

where ‘ $d$ ’—interplanar spacing, ‘ $a$ ’ & ‘ $c$ ’ are the lattice constants and  $h, k, l$  are the Miller indices of the planes. It is evident that as the doping increases, the lattice parameters remain slightly changed.

#### 3.2 Surface morphology and elemental mapping analysis

Figure 2a–d displays the typical morphological micrographs of the ZnO thin films with various contents of Cd (1 wt%, 3 wt%, and 5 wt%) a standard magnification (1  $\mu\text{m}$ ). These images show that the shape and morphology of ZnO films changes with increase in Cd concentrations. The well-known nano flower structure of the pure ZnO thin film is displayed in Fig. 2a. Furthermore, the remarkable change in morphology through the attendance of cadmium contains the ZnO matrix reported in Fig. 2b–d. However, the

**Fig. 1** X-ray diffraction patterns of ZnO and Cd:ZnO films with different Cd-doping concentrations



number of cadmium species incorporated into the ZnO lattice increased, the nano flower topography was gradually modified and transformed into a mixed agglomerated morphology. These findings are consistent with XRD tests, which show that the grain size of the film increases as the Cd concentration increases.

The compositional and elemental mapping analysis was done by the energy-dispersive (EDS) spectrum and is shown in Fig. 3a–e. Figure 3b–d shows the elemental mapping in various colors for O (red), Cd (green), and Zn (yellow). As shown in Fig. 3a, Zn and O have higher densities than Cd, and the films have a uniform distribution of Cd, Zn, and O. The EDS spectrum of Cd:ZnO (wt 5%) films were described in Fig. 3e. The presence of expected elements such as Zn, O, and Cd was detected in the prepared film, as shown in the figure. No other compounds rather Zn, O, and Cd were identified in the spectra, suggesting the purity of the Cd:ZnO films.

### 3.3 Optical studies

The absorbance spectra of ZnO and Cd:ZnO (1 wt%, 3 wt%, and 5 wt%) thin films coated over a glass substrate were measured at wavelengths ranging from 350 to 800 nm as shown in Fig. 4a. The addition of Cd to ZnO enhanced the optical absorption in all UV regions. Furthermore, by analyzing the dependence of the absorption factor on photon energy in the high absorption regions, the bandgap information of samples was estimated [30]. Figure 4b illustrates the optical band gap spectra of the synthesized film with various concentrations of Cd (0 wt%, 1 wt%, 3 wt%, and 5 wt%). The graph plotted between the photon energy ( $h\nu$ ) in the x-axis and  $(\alpha h\nu)^2$  in the y-axis. The optical band gap ( $E_g$ ) films were evaluated using the Tauc equation [31, 32]

$$(\alpha h\nu)^2 = A(h\nu - E_g) \quad (7)$$

where,  $E_g$ —optical band gap,  $h\nu$ —incident photon energy,  $A$ —a proportionality constant, and  $\alpha$ —absorption coefficient. The calculated bandgap values of ZnO and Cd:ZnO thin films are reported in Table 1. The band gap of ZnO film was calculated to be 3.03 eV, while that of Cd:ZnO (1 wt%, 3 wt%, and 5 wt%) films were 3.0 eV, 2.96 eV, and 2.95 eV, respectively. The decreasing bandgap in Cd:ZnO (1 wt%, 3 wt%, and 5 wt%) can be mainly ascribed to two factors (i) either the shift in bands energy levels or (ii) the creation of impurity levels between the conduction and valence band. The metallic doping generally creates more electrons in the oxide-based semiconductors and decreases the oxygen vacancy present in the intrinsic ZnO. Thus, the number of Zn–O bonds will increase due to the improved oxygen sites, which consequently increases the bond angle of Zn–O–Zn [33]. The increase in bond angle will enforce more symmetry in the ZnO lattice, which typically increases the bandwidth of conduction and valence bands which shrinks the bandgap. The Cd-doped film produces a minimum bandgap which is suitable for maximum light absorption. As a result, the enhancement of red shift and decrease in band gap energy ( $E_g$ ) confirm the presence of Cd<sup>2+</sup> inside the Zn<sup>2+</sup> site of the ZnO lattice.

### 3.4 Photoluminescence studies

The photoluminescence (PL) spectroscopy provides valuable information about the purity and quality of materials. The recorded photoluminescence spectra of ZnO and Cd:ZnO thin films at various molar concentrations (1 wt%, 3 wt%, and 5 wt%) with an

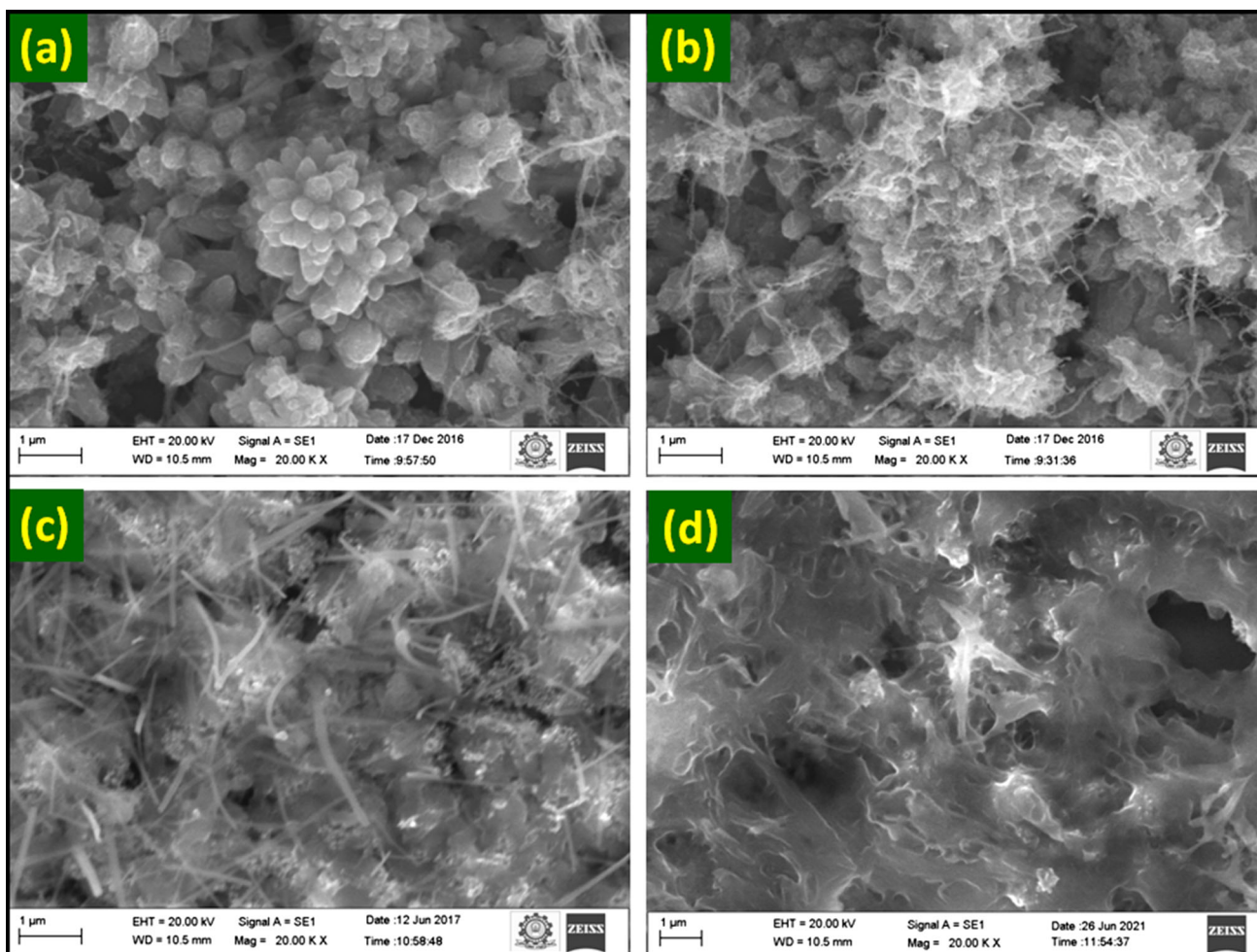


Fig. 2 a–d SEM images of the prepared ZnO and different wt% of Cd:ZnO thin films

excitation wavelength of 325 nm and an emission spectrum ranging from (400 to 600 nm) were exposed by Fig. 5. The emission peaks were detected at visible light regions in all of the deposited samples. The visible light emission peaks are located at 414, 430, 490, and 505 nm. In general, visible light emissions in ZnO thin films are caused by structural defects such as zinc interstitials, zinc vacancies, oxygen interstitials, and oxygen vacancies [34]. The ZnO and Cd:ZnO films give rise to the same emission band located at 414 nm, but the intensity has been changed. This may be due to fact that all the films were synthesized under the same conditions. The peak intensities increase with the doping percentage. The higher energy bands are attributed to the surface impurities or defect-related emissions such as oxygen vacancies and some interstitial oxygen, respectively. The intensity and position of this PL emission are also affected by Cd doping. Moreover, the sharp emission bands found in the spectra at 490 nm are attributed to the electronic transition possibility from the donor level of zinc interstitial ( $Zn_i$ ) to the acceptor level of zinc vacancy ( $V_{Zn}$ ), as the coexistence of these two defects is quite probable. The peak located at 505 nm is contributed to the oxygen vacancies [35].

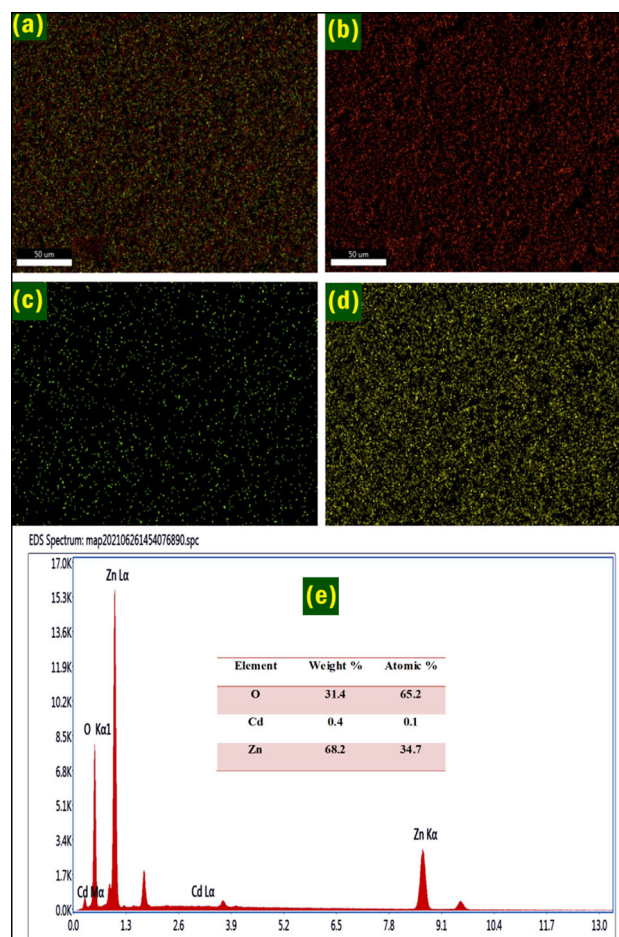
### 3.5 Raman spectroscopy studies

Raman spectroscopy is a useful technique for determining the Raman active modes of polar and nonpolar compounds. The synthesized ZnO and Cd:ZnO thin films in the presence of different dopant (1 wt%, 3 wt%, and 5 wt%) content were evaluated through Raman spectroscopy studies, where the spectral profile due to vibrational modes within the wavelength ranges from 200 to 800 nm at room temperature is presented in Fig. 6. Here,  $E_2^{high}$ ,  $A_1$  (LO) are the most evident vibrational modes. Based on the group theory, the wurtzite nanostructure of ZnO belongs to the  $C_{6v}$  space group with six active modes of vibrational modes  $E_{2L}$ ,  $E_{2T}$ ,  $A_{1T}$ ,  $A_{1L}$ ,  $E_{1T}$ ,  $E_{1L}$  (both LO and TO modes) due to the corresponding symmetry operation as follows [36]

$$\Gamma_{\text{Raman+infrared}}(P6_3mc) = 1A_1 + 2B_1 + 1E_1 + 2E_2 \tag{8}$$

where  $B_1$  is a silent mode of vibration.  $E_1$ ,  $A_1$  considers the polar modes of vibrations, and  $E_2^{high}$  and  $E_2^{low}$  are the nonpolar modes of vibration. The Raman spectra display different vibrational modes are observed at  $340\text{ cm}^{-1}$ ,  $392\text{ cm}^{-1}$ ,  $438\text{ cm}^{-1}$ , and  $576\text{ cm}^{-1}$ .

**Fig. 3 a–d** Overall elemental mapping images of the Cd:ZnO (wt 5%) thin films and **e** EDS spectrum of ZnO and wt 5% of Cd:ZnO thin films



The predominant peak at  $438\text{ cm}^{-1}$  is the characteristic  $E_2^{\text{high}}$  peak of ZnO and is mainly due to the vibration of oxygen atoms [37]. The presence of the most intense and higher peak  $E_2^{\text{high}}$  mode confirms the wurtzite structure with good crystallinity. The peak located at  $576\text{ cm}^{-1}$  is assigned to the longitudinal optical mode  $A_1$  (LO). Furthermore, we observe the presence of peaks corresponding to  $392$  and  $340\text{ cm}^{-1}$ , which represent the  $A_1$  (TO) mode and  $E_1$  (TO), respectively. The presence of Cd dopant in the ZnO lattice can cause a significant shift in the  $E_2^{\text{high}}$  mode's Raman vibrational frequency. The impurity ions produce more oxygen vacancies in  $E_2^{\text{high}}$  and reduce its corresponding band intensity compared to the pure one. The oxygen vacancy created by the cadmium atoms is one of the reasons for the lower intensity of the Raman shift. These factors achieve the better photocatalytic performance of the prepared films [38].

### 3.6 Photocatalytic studies

In this study, they evaluated the photocatalytic activity of the synthesized ZnO and Cd:ZnO thin films (1 wt%, 3 wt%, and 5 wt%) reported by the decomposition of methylene blue under UV light irradiation with different time intervals (0–150 min). Figure 7a–d displays the photodegradation process results in terms of the absorbance at wavelengths ranging from 400 to 800 nm. From the absorbance plots, we conclude that all the doped samples show greater photodegradation efficiency compared to the pure ZnO thin film due to the shift of the absorbance edges. So, the decrement identified for the Cd:ZnO catalysts was quicker than for pure ZnO, indicating that ( $\text{Cd}^{2+}$ ) ions significantly enhance ZnO photocatalytic activity. The degradation efficiencies of MB of the films were estimated by using Eq. (9) [39]

$$\eta = 1 - \frac{C}{C_0} \times 100\% \quad (9)$$

where  $C_0$  and  $C$  are the concentrations of the dye molecules under dark and light conditions. The photodegradation efficiency was calculated using Eq. (9), the graph was plotted between efficiency and irradiation time for ZnO and Cd:ZnO thin films under UV light irradiations. The degradation efficiencies of the ZnO and Cd:ZnO catalyst are displayed in Fig. 8. All the doped samples performed better degradation activity than the pure ZnO catalyst. After 150 min of light irradiation, the degradation efficiencies of the 0 wt%, 1 wt%, 3 wt%, and 5 wt% Cd:ZnO catalysts were 49.6%, 55.2%, 71.4%, and 82.5%, respectively [40]. The residual amount of MB

**Fig. 4 a** Absorbance spectra of ZnO and Cd:ZnO thin films and **b** Optical band gap values of ZnO and Cd:ZnO thin films

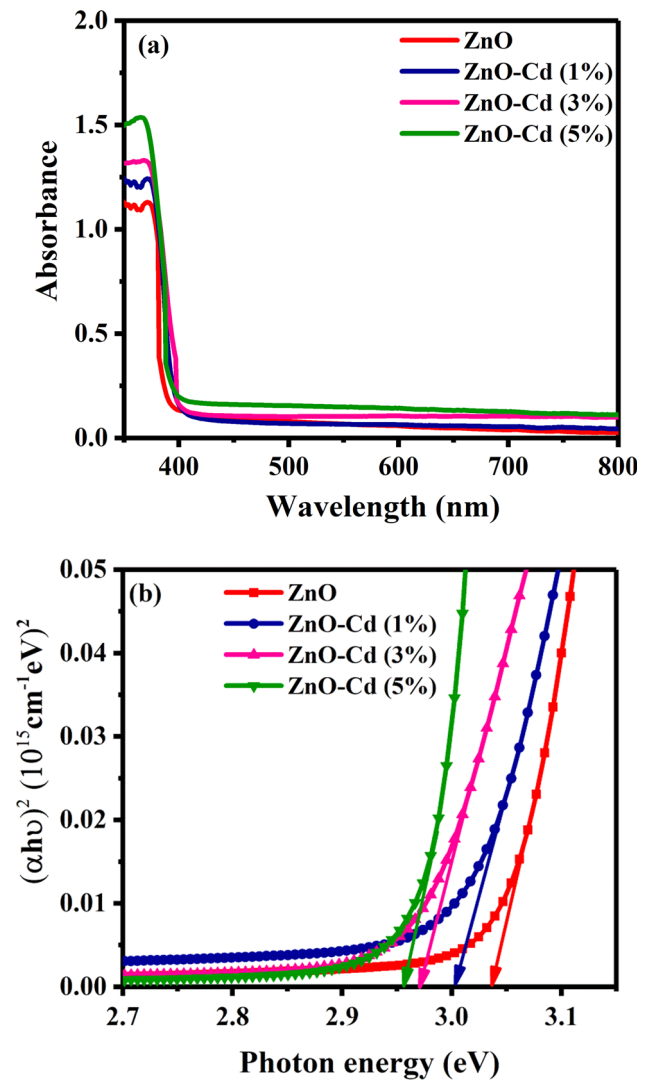


**Fig. 5** Photoluminescence spectrum of ZnO and different wt% of Cd:ZnO thin films

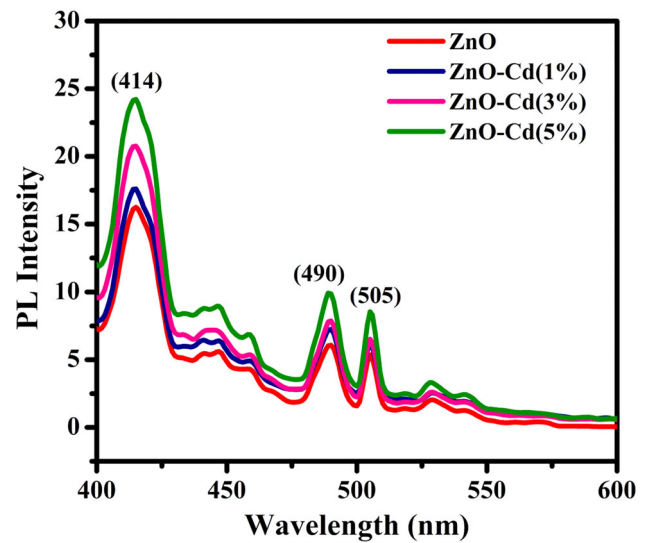


**Fig. 6** Raman spectra of ZnO and different wt% of Cd:ZnO thin films

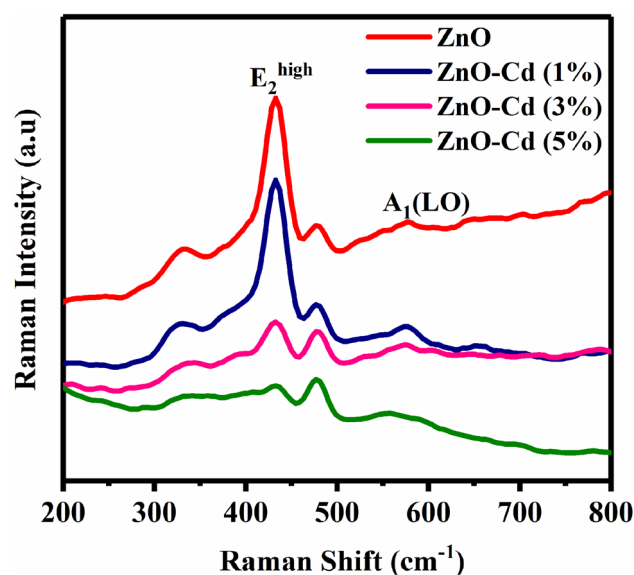


**Table 2** The calculated values of  $C/C_0$  of MB for ZnO and Cd:ZnO photocatalysts

Sample	Time interval					
	0 min	30 min	60 min	90 min	120 min	150 min
ZnO	1	0.996	0.9504	0.8895	0.8289	0.7044
Cd:ZnO (1%)	1	0.991	0.925	0.8266	0.7696	0.6562
Cd:ZnO (3%)	1	0.9265	0.8205	0.7435	0.5819	0.3635
Cd:ZnO (5%)	1	0.8442	0.7053	0.4853	0.3466	0.1904

dye after photodegradation was measured using the plots of  $C/C_0$  is shown in Table 2. The photocatalytic degradation kinetics of the ZnO and Cd:ZnO catalysts were explored using the pseudo-first-order kinetic model suggested by Langmuir–Hinshelwood as follows [41]

$$K = \frac{\ln(C_0/C)}{t} \quad (10)$$

where  $K$  denotes the apparent rate constant and  $t$  denotes the time of irradiation. Plots of  $\ln(C_0/C)$  versus irradiation time of MB in the presence of ZnO and Cd:ZnO catalysts are shown in Fig. 9. The degradation of MB dye in the absence of catalysts is almost negligible, and the  $\ln C_0/C$  values rise with reaction time after exposing the mixed solution of MB dye with ZnO and Cd:ZnO catalysts to UV light. The  $K$  values of the ZnO and Cd:ZnO (1 wt%, 3 wt%, and 5 wt%) thin films were 0.007, 0.009, and 0.010  $\text{min}^{-1}$ , respectively. The hexagonal structure of the doped Zn provided more surface area while also increasing surface defects. Because of these factors, the Cd:ZnO (wt% 5) catalyst had more active sites, which allowed it to excite more photoinduced electron and hole pairs under UV light, resulting in increased photocatalytic efficiency.

### 3.7 Photocatalytic mechanism

The photocatalytic activity is known to be affected by many factors, including the light absorption capacity, separation efficiency of photogenerated electrons and holes, and photogenerated hole oxidation ability. Figure 10 shows the photocatalytic mechanism, which involves charge transfer during the degradation of MB dye by the Cd-doped ZnO catalyst. Under visible light illumination, electrons in the semiconductor (SC) jump from the valence band (VB) to the conduction band (CB). Cd is an SC with a narrow bandgap (2.1 eV), whereas with the broad band gap of anatase ZnO (3.37 eV) [42–44]. Electrons in the VB of cadmium can be stimulated to the CB by visible light, causing holes in the VB. By contrast, a small number of electrons in ZnO could be stimulated from the VB to the CB. The photoinduced electrons in the cadmium CB are shifted to the ZnO CB, which serves as a photoelectron receiver. The electrons can be captured by oxygen ( $\text{O}_2$ ) and converted to superoxide radical anions ( $\bullet\text{O}_2^-$ ), which can then react with a contaminant. Furthermore, the holes in the cadmium VB can react with  $\text{H}_2\text{O}$  to form hydroxyl radicals, which can then react with the dye [45]. In photocatalytic reactions, these reactive radicals can efficiently convert MB to  $\text{H}_2\text{O}$  and  $\text{CO}_2$ , as well as other harmless molecules.



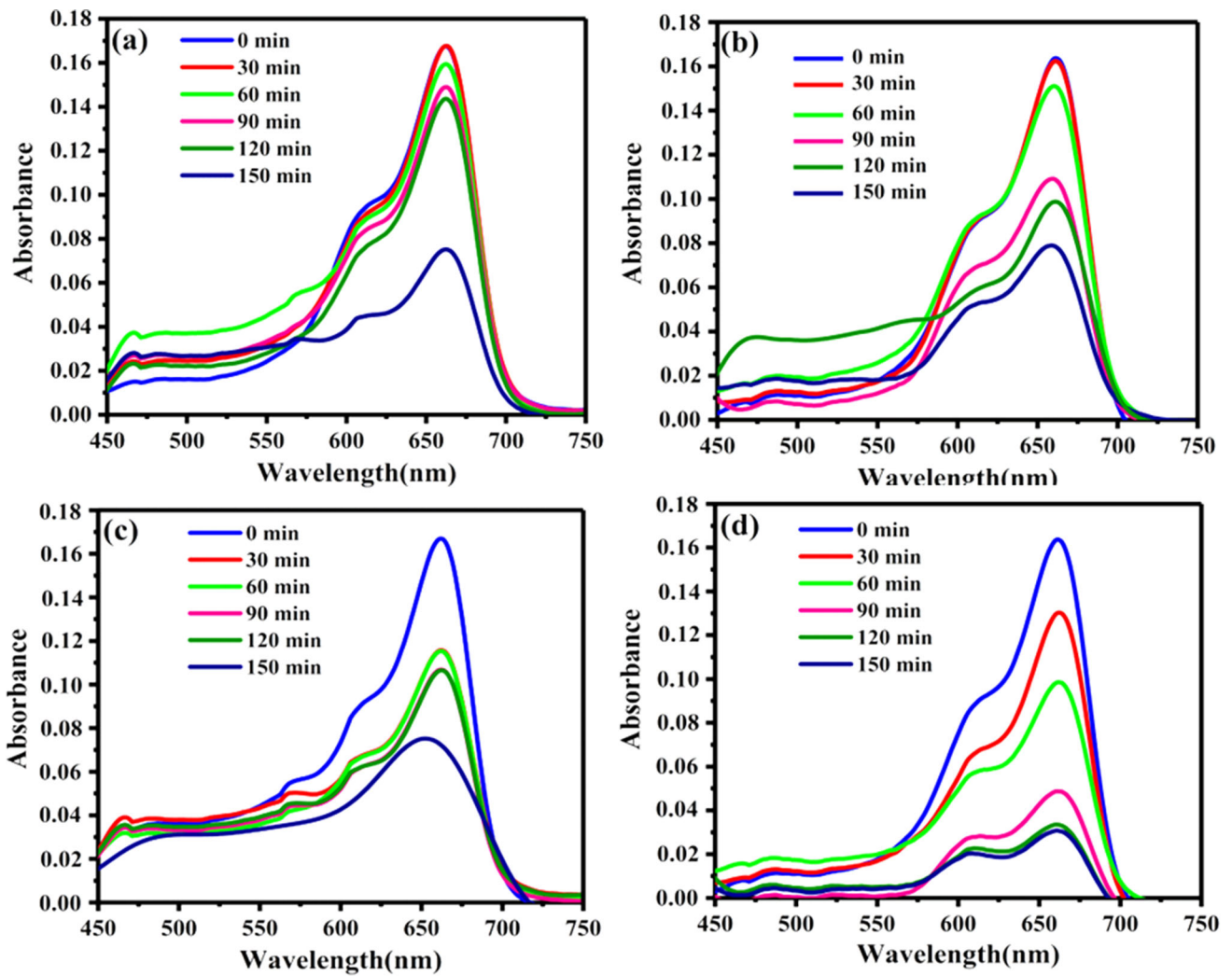
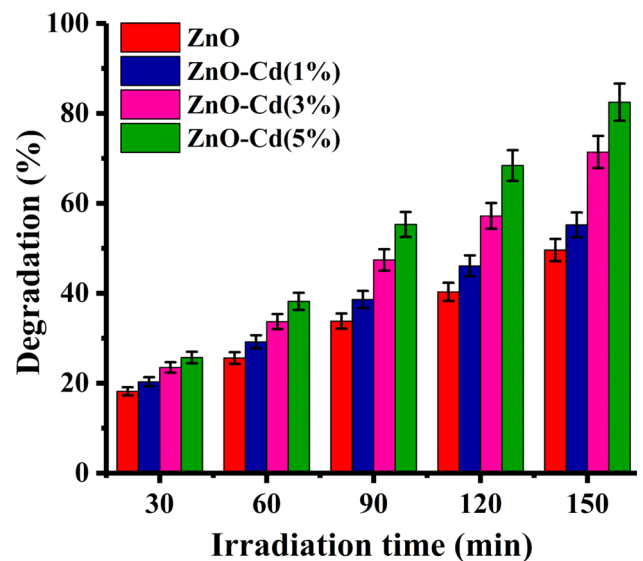
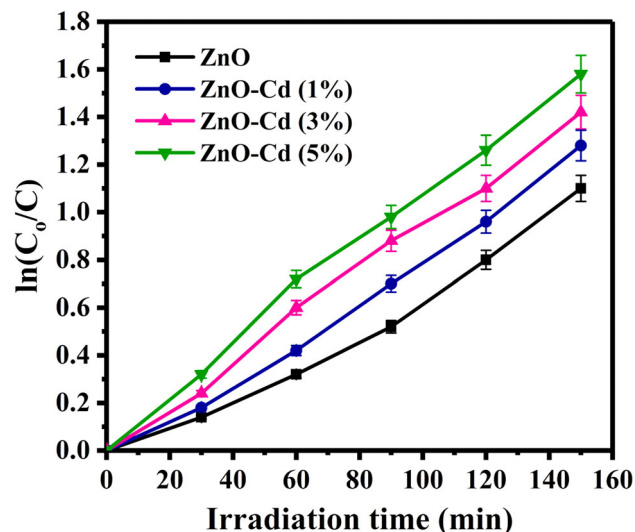


Fig. 7 Absorbance spectra of a ZnO, b Cd:ZnO (wt 1%), c Cd:ZnO (wt 3%), d Cd:ZnO (wt 5%) catalyst

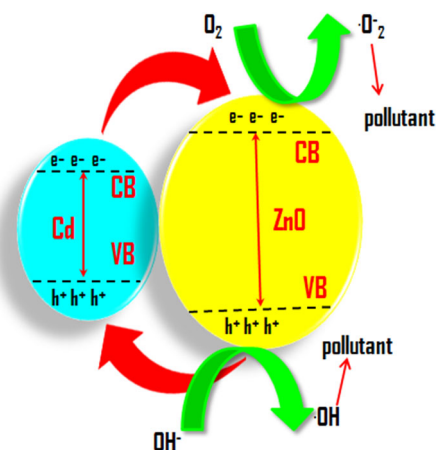
Fig. 8 Photodegradation efficiency of ZnO and Cd:ZnO catalyst



**Fig. 9** Plots of  $\ln(C_0/C)$  versus irradiation time of the MB for ZnO and Cd:ZnO photocatalysts



**Fig. 10** Photocatalytic charge transfer mechanism during dye MB degradation by Cd:ZnO catalyst



Finally, recombination takes place after the photodegradation process. The following expressions describe the photocatalytic process under ultraviolet radiation [45–47]



The expressions (11–12) refer to what commonly occurs in the ZnO thin films. The additional expressions (15–17) occurred when the Cd:ZnO doped films performed the photodegradation process.



#### 4 Conclusion

In summary, the ZnO and Cd:ZnO (1–5 wt%) thin films were successfully synthesized using a modified SILAR approach and deposited on silicon glass substrates. Various characterization techniques are used to investigate the synthesized films. The crystalline nature of the obtained ZnO and Cd:ZnO films was confirmed by XRD studies with the strong orientation peak of (002) as well as

the  $E_2^{\text{high}}$  mode presented in Raman studies. The substitution of  $\text{Cd}^{2+}$  ions on the ZnO lattice was confirmed through the SEM and elemental mapping analysis. The optical studies confirm that as the Cd doping percentage increases, the band gap energy decreases, and the optical band gap energy of the films decreases from 3.03 to 2.95 eV. The Cd-doped ZnO films exhibited better photocatalytic efficiency compared to that of pure ZnO. In this study, 5 wt% Cd-doped ZnO demonstrated the highest photocatalytic performance of 82.5% within 150 min. As a result, a reliable and cost-effective Cd:ZnO catalyst has emerged as a promising candidate in the field of environmental applications.

**Author contributions** MS is first author and was involved in conceptualization, methodology, investigation; writing—original draft, formal analysis. GS helped in methodology, validation, visualization. KK contributed to validation, resources, writing—reviewing and editing. SU was involved in formal analysis, methodology. PB helped in methodology, validation, visualization. MK is the corresponding author and helped in validation, visualization, supervision.

**Data Availability Statement** This manuscript has associated data in a data repository. [Authors' comment: The data that support the findings of this study are available from the corresponding author upon reasonable request.]

## Declarations

**Conflict of interest** The authors declare that they have no conflict of interest.

## References

- M.Z. WeiYunwei, W.S. ShujuanLyu, O.-P. ShuqiangLyu, ligand-free, room-temperature synthesis of Au/Pd/ZnO nanoclusters with ultra-low noble metal loading and synergistically improved photocatalytic performances. *RSC Adv.* **11**(37), 22618–22624 (2021). <https://doi.org/10.1039/D1RA02958D>
- F. SanadMohamed, A. EsmailShalan, M.A. Ahmed, M.F. Abdel Messih, The controlled synthesis and DFT investigation of novel (0D)–(3D) ZnS/SiO<sub>2</sub> heterostructures for photocatalytic applications. *RSC Adv.* **11**, 22352–22364 (2021). <https://doi.org/10.1039/D1RA02284A>
- K.H. PoornimaSengunthar, C. Bhavsar, U.S. Balasubramanian, Joshi, Physical properties and enhanced photocatalytic activity of ZnO-rGO nanocomposites. *Appl. Phys. A* **126**(7), 567 (2020). <https://doi.org/10.1007/s00339-020-03753-6>
- A. Fouda, S.S. Salem, A.R. Wassef, M.F. Hamza, T.I. Shaheen, Optimization of green biosynthesized visible light active CuO/ZnO nano-photocatalysts for the degradation of organic methylene blue dye. *Heliyon* **6**(9), e04896 (2020). <https://doi.org/10.1016/j.heliyon.2020.e04896>
- M. Perez-Gonzalez, S.A. Tomas, J. Santoyo-Salazar, S. Gallardo-Hernandez, M.M. Tellez-Cruz, O. Solorza-Feria, Sol-gel synthesis of Ag-loaded TiO<sub>2</sub>-ZnO thin films with enhanced photocatalytic activity. *J. Alloys Compd.* **779**, 908–917 (2019). <https://doi.org/10.1016/j.jallcom.2018.11.302>
- R. Katala, S. Masudy-Panah, M. Sabbaghanb, Z. Hossaini, M.H. Farahani, Photocatalytic degradation of triclosan by oxygen defected CuO thin film. *Sep. Purif. Technol.* **250**, 117239 (2020). <https://doi.org/10.1016/j.seppur.2020.117239>
- M.K. Singha, A. Patra, V. Rojwal, K.G. Deepa, Single-step fabrication of ZnO microflower thin films for highly efficient and reusable photocatalytic activity. *J. Mater. Sci. Mater.* **31**(16), 13578–13587 (2020). <https://doi.org/10.1007/s10854-020-03914-6>
- A.E. Putri, L. Roza, S. Budi, A.A. Umar, V. Fauzia, Tuning the photocatalytic activity of nanocomposite ZnO nanorods by shape-controlling the bimetallic AuAg nanoparticles. *Appl. Surf. Sci.* **536**, 147847 (2021). <https://doi.org/10.1016/j.apsusc.2020.147847>
- K. Sahu, S. Choudhary, S. Mohapatra, Fabrication of Au-CuO hybrid plasmonic nanostructured thin films with enhanced photocatalytic activity. *Mater. Res. Bull.* **123**, 110707 (2020). <https://doi.org/10.1016/j.materresbull.2019.110707>
- A. Nicosia, F. Vento, G.M.D. Mari, L. D'Urso, P.G. Mineo, TiO<sub>2</sub>-based nanocomposites thin film having boosted photocatalytic activity for xenobiotics water pollution remediation. *Nanomaterials* **11**, 400 (2021). <https://doi.org/10.3390/nano11020400>
- P.R. Chithira, T.T. John, Correlation among oxygen vacancy and doping concentration in controlling the properties of cobalt doped ZnO nanoparticles. *J. Magn. Magn. Mater.* **496**, 165928 (2020). <https://doi.org/10.1016/j.jmmm.2019.165928>
- R. Saravanan, H. Shankar, T. Prakash, V. Narayanan, A. Stephen, ZnO/CdO composite nanorods for photocatalytic degradation of methylene blue under visible light. *Mater. Chem. Phys.* **125**, 277–280 (2011). <https://doi.org/10.1016/j.matchemphys.2010.09.030>
- D. Tekin, H. Kiziltas, H. Urgan, Kinetic evaluation of ZnO/TiO<sub>2</sub> thin film photocatalyst in photocatalytic degradation of orange G. *J. Mol. Liq.* **306**, 112905 (2020). <https://doi.org/10.1016/j.molliq.2020.112905>
- R. Mohan, K. Ravichandran, A. Nithya, K. Jothivenkatachalam, C. Ravidhas, B. Sakthivel, Influence of spray flux density on the photocatalytic activity and certain physical properties of ZnO thin films. *J. Mater. Sci. Mater. Electron.* **25**, 2546–2553 (2014). <https://doi.org/10.1007/s10854-014-1908-0>
- L. Roza, Y. Febrianti, S. Iwan, V. Fauzia, The role of cobalt doping on the photocatalytic activity enhancement of ZnO nanorods under UV light irradiation. *Surf. Interfaces* **18**, 100435 (2020). <https://doi.org/10.1016/j.surfin.2020.100435>
- G.T. Rao, R.V.S.S.N. Ravikumar, Novel Fe-doped ZnO-CdS nanocomposite with enhanced visible light-driven photocatalytic performance. *Mater. Res. Innov.* **25**(4), 215–220 (2021). <https://doi.org/10.1080/14328917.2020.1774726>
- R.I. Muhammad, M.G. Azam, Enhanced photocatalytic activity of Mg-doped ZnO thin films prepared by sol-gel method. *Surf. Eng.* **37**, 775–783 (2021). <https://doi.org/10.1080/02670844.2020.1801143>
- W. Vallejo, A. Cantillo, C. Diaz-Urbe, Methylene blue photo degradation under visible irradiation on Ag-doped ZnO thin films. *Int. J. Photoenergy* **2020**, 11 (2020). <https://doi.org/10.1155/2020/1627498>
- E.S. Kholoud, A.M. Mokhtar, I. Soliman, M. Ramadan, B.S. Shaheen, N.K. Allam, Ge-doped ZnO nanorods grown on FTO for photoelectron chemical water splitting with exceptional photo conversion efficiency. *Int. J. Hydrog. Energy* **46**(1), 209–220 (2021). <https://doi.org/10.1016/j.ijhydene.2020.09.208>
- R. Pandya, H. Patel, N.A. Shah, P.S. Solanki, Y.N. Jani, M.J. Keshvani, Substitutional effect of copper replacement by cadmium on structural, microstructural and electrical properties of Cu<sub>1-x</sub>Cd<sub>x</sub>O oxides. *Mater. Today Commun.* **25**, 101458 (2020). <https://doi.org/10.1016/j.mtcomm.2020.101458>
- M.R. Bindhu, K. Ancy, M. Umadevi, G.A. Esmail, N.A. Al-Dhabi, M.V. Arasu, Synthesis and characterization of zinc oxide nanostructures and its assessment on enhanced bacterial inhibition and photocatalytic degradation. *J. Photochem. Photobiol. B* **210**, 111965 (2020). <https://doi.org/10.1016/j.jphotobiol.2020.111965>
- G. Poongodi, P. Anandan, R.M. Kumar, R. Jayavel, Studies on visible light photocatalytic and antibacterial activities of nanostructured cobalt doped ZnO thin films prepared by sol-gel spin coating method. *SAA* **148**, 237–243 (2015). <https://doi.org/10.1016/j.saa.2015.03.134>

23. K. Kasirajan, L. Bruno Chandrasekar, S. Maheswari, M. Karunakaran, P. Shunmuga Sundaram, A comparative study of different rare-earth (Gd, Nd, and Sm) metals doped ZnO thin films and its room temperature ammonia gas sensor activity: Synthesis, characterization, and investigation on the impact of dopant. *Opt. Mater.* **121**, 111554 (2012). <https://doi.org/10.1016/j.optmat.2021.111554>
24. U.D. Babar, N.M. Garad, A.A. Mohite, B.M. Babar, H.D. Shelke, P.D. Kamble, U.T. Pawar, Study the photovoltaic performance of pure and Cd-doped ZnO nanoparticles prepared by reflux method. *Mater. Today* **43**, 2780–2785 (2021). <https://doi.org/10.1016/j.matpr.2020.08.008>
25. S.P. Bharath, K.V. Bangera, G.K. Shivakumar, Effect of cadmium incorporation on the properties of zinc oxide thin films. *Appl. Nanosci.* **8**(1), 187–193 (2018). <https://doi.org/10.1007/s13204-018-0661-8>
26. S. Maheswari, M. Karunakaran, K. Hariprasad, K. Kasirajan, I.L.P. Raj, L.B. Chandrasekar, T. Alshahrani, M. Shkir, S. AlFaify, Noticeable enhancement in NH<sub>3</sub> sensing performance of nebulizer spray pyrolysis deposited SnO<sub>2</sub> thin films: an effect of Tb doping. *Superlattices Microstruct.* **154**, 106868 (2021). <https://doi.org/10.1016/j.spmi.2021.106868>
27. K.R. Devi, G. Selvan, M. Karunakaran, K. Kasirajan, L.B. Chandrasekar, M. Shkir, S. AlFaify, SILAR-coated Mg-doped ZnO thin films for ammonia vapor sensing applications. *J. Mater. Sci. Mater.* **31**, 10186–10195 (2020). <https://doi.org/10.1007/s10854-020-03564-8>
28. K.R. Devi, G. Selvan, K.H. Prasad, M. Karunakaran, K. Kasirajan, V. Ganesh, S. AlFaify, Effect of Cu<sup>2+</sup> doping on the structural, optical, and vapor-sensing properties of ZnO thin films prepared by SILAR method. *J. Mater. Sci. Mater.* **31**(19), 16548–16560 (2020). <https://doi.org/10.1007/s10854-020-04210-z>
29. J. Zhang, S.-Q. Zhao, K. Zhang, J.-Q. Zhou, Y.-F. Cai, A study of photoluminescence properties and performance improvement of Cd-doped ZnO quantum dots prepared by the sol–gel method. *Nanoscale Res. Lett.* **7**(405), 1–7 (2012). <https://doi.org/10.1186/1556-276X-7-405>
30. A.J. Jebathew, M. Karunakaran, R. Ade, N.D. Jayram, V. Ganesh, Y. Bitla, S. Vinoth, H. Algarni, I.S. Yahia, Optical manipulation of nebulizer spray pyrolysed ZnS thin films for photodetector applications: effect of Al, Sn and Sb doping. *Opt. Mater.* **117**, 111177 (2021). <https://doi.org/10.1016/j.optmat.2021.111177>
31. A.M. Khudheir, A.H. Abdulsada, H.G. Rashid, H.L. Mansour, H.S. Rasheed, H.H. Murbat, N.F. Habubi, Non-thermal plasma effects on structural and optical properties of Cd doped ZnO thin films. *IOP Conf. Ser. Mater. Sci. Eng.* **871**, 012061 (2020). <https://doi.org/10.1088/1757-899x/871/1/012061>
32. K.P. Raj, K. Sadaiyandi, A. Kennedy, S. Sagadevan, Z.Z. Chowdhury, M. Johan, R. Bin, F.A. Aziz, R.F. Rafique, R.T. Selvi, R. Rathinabala, Influence of Mg doping on ZnO nanoparticles for enhanced photocatalytic evaluation and antibacterial analysis. *Nanoscale Res. Lett.* **13**, 229 (2018). <https://doi.org/10.1186/s11671-018-2643-x>
33. K. Ravichandran, K.S. Seelan, M.M. Ibrahim, P. Kavitha, Improved solar light responsive photocatalytic activity of ZnO: W films: effect of W loading level. *Mater. Today Proc.* (2020). <https://doi.org/10.1016/j.matpr.2020.06.527>
34. C. Dhanraj, K. Ravichandran, P. Kavitha, P.K. Praseetha, Excess free-electrons activated photocatalytic ability of ZnO films through co-doping of higher oxidation state transition metals Ta and Mo. *Inorg. Chem. Commun.* **118**, 107986 (2020). <https://doi.org/10.1016/j.inoche.2020.107986>
35. P. Saxena, P. Choudhary, A. Yadav, B. Dewangan, V.N. Rai, A. Mishra, Improved structural and dielectric properties of Cd and Ti dual doped ZnO nanoparticles. *Appl. Phys.* **126**(765), 11 (2020). <https://doi.org/10.1007/s00339-020-03943-2>
36. N. Rana, S. Chand, A.K. Gathania, Tailoring the structural and optical properties of ZnO by doping with Cd. *Ceram. Int.* **41**(9), 12032–12037 (2015). <https://doi.org/10.1016/j.ceramint.2015.06.017>
37. Z.R. Khan, A.S. Alshammari, M. Bouzidi, M. Gandouzi, M. Shkir, S. Alfaify, Emission and opto-dielectric nonlinearity in 2D Cd–ZnO–Na nanostructures: an effect of Na doping. *J. Mater. Sci. Mater.* **31**, 12116–12126 (2020). <https://doi.org/10.1007/s10854-020-03758-0>
38. G. Shanmugavel, A.R. Balu, V.S. Nagarethinam, S. Ravishankar, M. Suganya, S. Balamurugan, K. Usharani, C. Kayathiri, M. Karthika, CdO: Ag thin films with enhanced visible light photocatalytic activity against metanil yellow. *SN Appl. Sci.* (2019). <https://doi.org/10.1007/s42452-019-1237-2>
39. Y. Wu, N. Luo, R. Xie, Rodlike cadmium-incorporated zinc tungstate nanoarchitecture fabricated by a facile and template-free strategy as a photocatalyst for the effective degradation of organic pollutants in sewage. *ACS Omega* **5**(38), 24318–24328 (2020). <https://doi.org/10.1021/acsomega.0c02541>
40. S. Anbarasu, S. Ilangoan, K. Usharani, A. Prabhavathi, M. Suganya, M. Karthika, C. Kayathiri, S. Balamurugan, A.R. Balu, Realization of improved visible light-mediated photocatalytic activity of Al<sub>2</sub>O<sub>3</sub> nanoparticles through cobalt doping. *J. Electron. Mater.* **49**(1), 869–879 (2020). <https://doi.org/10.1007/s11664-019-07759-6>
41. P. GhoderaoKaruna, S.N. Jamble, R.B. Kale, Hydrothermally synthesized Cd-doped ZnO nanostructures with efficient sunlight-driven photocatalytic and antibacterial activity. *J. Mater. Sci. Mater.* **30**(12), 11208–11219 (2019). <https://doi.org/10.1007/s10854-019-01466-y>
42. P. Dumrongrojthanath, A. Phuruangrat, S. Thongtem, T. Thongtem, Photocatalysis of Cd-doped ZnO synthesized with precipitation method. *Rare Met.* **40**(3), 537–546 (2021). <https://doi.org/10.1007/s12598-019-01283-6>
43. W. Vallejo, A. Cantillo, B. Salazar, C. Diaz-Urbe, W. Ramos, E. Romero, M. Hurtado, Comparative study of ZnO thin films doped with transition metals (Cu and Co) for methylene blue photodegradation under visible irradiation. *Catalysts* **10**(5), 528 (2020). <https://doi.org/10.3390/catal10050528>
44. X. Chungping, P.R. Anusuyadevi, C. Aymonier, R. Luque, S. Marre, Nanostructured materials for photocatalysis. *Chem. Soc. Rev.* **48**, 3868–3902 (2019). <https://doi.org/10.1039/C9CS00102F>
45. A.K. Azfar, M.F. Kasim, I.M. Lokman, H.A. Rafeaie, M.S. Mastuli, Comparative study on photocatalytic activity of transition metals (Ag and Ni)-doped ZnO nanomaterials synthesized via sol–gel method. *R. Soc. Open Sci.* **7**, 191590 (2020). <https://doi.org/10.1098/rsos.191590>
46. G. El Fidha, N. Bitri, F. Chaabouni, S. Acosta, F. Güell, C. Bittencourt, J. Casanova-Chafer, E. Llobet, Physical and photocatalytic properties of sprayed Dy doped ZnO thin films under sunlight irradiation for degrading methylene blue. *RSC Adv.* **11**, 24917–24925 (2021). <https://doi.org/10.1039/D1RA03967A>
47. L.V. Trandafilović, D.J. Jovanović, X. Zhang, S. Ptašniška, M.D. Dramićanin, Enhanced photocatalytic degradation of methylene blue and methyl orange by ZnO: Eu nanoparticles. *Appl. Catal. B* **203**, 740–752 (2017). <https://doi.org/10.1016/j.apcatb.2016.10.063>

Springer Nature or its licensor (e.g. a society or other partner) holds exclusive rights to this article under a publishing agreement with the author(s) or other rightsholder(s); author self-archiving of the accepted manuscript version of this article is solely governed by the terms of such publishing agreement and applicable law.